Charge Storage Mechanism of a Quinone Polymer Electrode for Zinc-ion Batteries

Journal of The Electrochemical Society, 2020 **167** 070558

Charge Storage Mechanism of a Quinone Polymer Electrode for Zinc-ion Batteries

Ye Zhang,[1,*] Yanliang Liang,[1,2] Hui Dong,[1] Xiaojun Wang,[1,2] and Yan Yao[1,2,,z]**

[1]*Department of Electrical and Computer Engineering and Materials Science and Engineering Program, University of Houston, Houston, Texas 77204, United States of America*
[2]*Texas Center for Superconductivity at the University of Houston, Houston, Texas 77204, United States of America*

The capability for a cathode material to store zinc ions is critical for the viability of an aqueous zinc-ion battery. This work investigates the charge storage mechanism of a quinone polymer via a combination of electrochemical quartz crystal microbalance with dissipation monitoring and in situ Fourier transform infrared spectroscopy. Non-hydrated zinc ions are found to be the cation species associated with the quinone-related redox reaction, while the counter anions also participate the reaction probably due to the unique p-dopable linker present in the polymer.

 [DOI: 10.1149/1945-7111/ab847a]

Manuscript submitted January 1, 2020; revised manuscript received March 24, 2020. Published April 9, 2020. *This paper is part of the JES Focus Issue on Challenges in Novel Electrolytes, Organic Materials, and Innovative Chemistries for Batteries in Honor of Michel Armand.*

Supplementary material for this article is available online

Aqueous zinc-ion batteries (AZIBs) offer a potentially stable alternative to alkaline rechargeable zinc batteries in utilizing zinc metals for low-cost and safe energy storage.[1,2] Two fundamental features of AZIBs are (1) near-neutral aqueous electrolytes, in which zinc dendrites growth is apparently suppressed compared with that in alkaline electrolytes, and (2) Zn^{2+}-storing cathode materials, which do not store protons in cathodes and maintain the near-neutral pH of an electrolyte throughout charge-discharge processes. Because of the importance of stored species at the cathode for the viability of a battery, the charge storage mechanism in cathode materials has been under scrutinization.[1,3] Among cathode materials proposed for high-energy AZIBs, many vanadium oxides seem to store zinc-ions, while manganese oxides more often than not involve proton storage which raises concerns of pH variation of the electrolyte.[4–6] Quinones have been recently proposed as versatile electrode materials for aqueous batteries.[7–9] Early attempts of quinones for AZIBs have resulted in promising specific energy and cycling stability.[10–13] It is therefore interesting to investigate the charge storage mechanism in these materials and assess their viability for practical applications.

This work focuses on the identification of stored ions in a quinone polymer, poly(benzoquinonyl sulfide) (PBQS), as an AZIB cathode material. Possible ions to be involved in the electrode reaction include zinc ions, protons, counter anions (in this case triflate), and their hydrated forms. Spectroscopic technologies suitable for qualitative and quantitative analyses of the electrode reaction of organic materials have undergone major development in recent years. Electrochemical quartz crystal microbalance (EQCM) is an established tool to quantitatively probe the stored ions in redox-active polymers and carbon materials.[14,15] Recent advancement with dissipation monitoring (EQCM-D) further strengthened the technique for characterizing softer electrodes.[16] On the other hand, Fourier transform infrared spectroscopy (FTIR) is a standard technique for qualitative detection of chemical groups, thus a useful tool to compliment EQCM-D which may lack chemical information. In situ FTIR has been proven effective in monitoring the electrode reactions in organic carbonyl electrodes, though the use for detection of stored ions has not been reported. Here we combine EQCM-D and FTIR techniques for a comprehensive understanding of the charge storage mechanism of PBQS in a near-neutral zinc electrolyte.

Experimental

PBQS was synthesized following the method reported in the literature.[17] The electrodes used in the EQCM-D study were prepared by a spray-coating method using an airbrush.[18,19] The PBQS powders, multiwall carbon nanotubes (>95%, US Research Nanomaterials), and Nafion (5 wt% in a mixture of lower aliphatic alcohols and water, Millipore Sigma) were dispersed in *N*-methyl-2-pyrrolidone (99.5%, Millipore Sigma) by ultrasonication with a mass ratio of 7:2:1. The well-dispersed slurry was then spray-coated onto a 5 MHz Au sensor (Biolin Scientific) and dried at 120 °C for 30 min.

Multi-harmonic EQCM-D were measured with an electrochemical module (QEM 401, Biolin Scientific) using a QCM-D system (Q-Sense E1, Biolin Scientific). The PBQS coated gold sensor (QSX 301, Biolin Scientific) served as the cathode and zinc foil (99.9%, Alfa Aesar) served as both the counter and reference electrode. Highly resistant Karlrez O-rings were used for sealing the cell. 130 ul electrolyte was pumped into the module and the testing temperature was kept constantly at 25 °C. The changes of frequency and dissipation were monitored in two modes: galvanostatic cycling at a current of 50 μA or cyclic voltammetry cycling at a scan rate of 10 mV s^{-1}. The change of frequency and dissipation of the 5th and 7th overtones were fitted with a Voigt model provided in the Qtool software.

In situ FTIR was measured with a FTIR spectrometer (Nicolet iS5, Thermo Scientific) with a custom-built cell. The electrode pellet was prepared by mixing PBQS, Kejent black and polytetrafluoroethylene with a mass ratio of 8:1:1. The pellet was first pressed against the diamond window followed by a stainless-steel mesh, a glass fiber separator, and a zinc foil. The electrolyte was 3 M $Zn(OTf)_2$ in deuterium oxide (D_2O, 99.9 atom.% D, Millipore Sigma). Replacing H_2O with D_2O avoids the complication of overlapping absorption bands of O−H and C=O in FTIR spectra.

Cycling performance of PBQS was tested in two-electrode coin cells (CR2032) using a zinc foil as the anode. The cathode slurry was prepared by hand-grinding PBQS, Kejent black and polytetrafluoroethylene in ethanol with a mass ratio of 7:2:1. The areal loading of active material is ~1 mg cm^{-2}. The electrolyte was 3 M $Zn(OTf)_2$ (98%, Millipore Sigma) in deionized water with the pH value of 4.0. Electrochemical characterizations were performed with a potentiostat (VMP3, Biologic).

Results and Discussion

EQCM-D study has been demonstrated effective for investigating the mass transport and mechanical properties of various inorganic

*Electrochemical Society Student Member.
**Electrochemical Society Member.
[z]E-mail: yyao4@uh.edu

electrodes[14,19–23] and organic radical polymers.[15] The active material is coated on a gold-coated quartz crystal sensor serving as a working electrode. By applying an alternating voltage between two gold electrodes at a fundamental frequency, the quartz crystal is forced to oscillate and display different overtones ($\Delta f/n$). During an electrochemical process, an increase in electrode mass decreases the oscillation frequency and the energy dissipated by the applied oscillatory shear wave is tracked by a dissipation monitor.[15] The change in frequency and dissipation could be fitted by various models depending on electrode geometry and morphology.[24] If the coating is stiff and porous and $\Delta f/n$ are n-dependent, a hydrodynamic model should be used.[20] If the coating is soft, a Voigt-type viscoelastic model should be used.[15] In either case, when the hydrodynamic or viscoelastic contribution is negligibly small, $\Delta f/n$ should be independent of n, and therefore a gravimetric model can be used for data fitting.[24]

Figure 1a shows the SEM image of a PBQS electrode coated on a gold sensor by spray-coating method. The film is uniform without obvious uncovered area on the gold sensor surface. Higher resolution image (Fig. 1b) reveals less than micrometer-sized PBQS particles and carbon nanotubes were well-dispersed forming a dense layer. The cross-sectional SEM shown in Fig. 1c reveals the flat and compact coating layer with a thickness around 200 nm. The areal mass loading of the composite film is 25 ug cm^{-2}. The coated sensor was assembled in a QEM 401 electrochemistry module (Fig. 1d) using a zinc foil as both the counter and reference electrode in a 3 M $Zn(OTf)_2$ aqueous electrolyte. Figure 1e shows the normalized frequency change ($\Delta f/n$) and resonance width peak ($\Delta W/n$) by the overtone order (n = 5, 7, 9) during a typical EQCM-D cycle. Because $\Delta f/n$ is independent of n and $\Delta W/n$ is close to zero, we conclude the contribution from the viscoelastic effect is negligible,[21] therefore the EQCM-D data can be fitted using the gravimetric model.

We investigated the EQCM-D responses under two operating conditions, galvanostatic cycling vs cyclic voltammetry cycling. Figure 2a shows the galvanostatic voltage profile of initial 11 cycles starting from a fresh electrode. Except for the first two cycles where ionic species trapping takes place (details will be discussed later), the change of f_3 within each cycle is reversible. We are able to calculate the specific capacity based on the mass of PBQS and plot the galvanostatic cycling data in Fig. 2b. The specific capacity of 220 mAh g^{-1} agrees with the capacity that measured from coin cells. Stable electrochemical performance indicates no dissolution typically observed for organic electrodes. To investigate the dominant reaction mechanism in details, we plot the EQCM-D response of a typical cycle (11th cycle in this case) in Fig. 2c. During the discharge process, the coated film increases in mass while decreases in dissipation. The decrease in dissipation (blue) suggests stiffening of the polymer film.[15,21] In the charge process, the mass and dissipation reverse, respectively. The mass change (red) is small at higher voltages and gradually increases when voltage is less than 1 V, indicating a voltage-dependent storage mechanism involving multiple charge species. The mass change per charge transfer ($\Delta m/e$), when voltage is less than 1 V, fits nicely with the theoretical $\Delta m/e$ value of Zn^{2+} (0.337 mg C^{-1}), indicating storage of naked Zn^{2+} instead of its hydrated forms. The smaller mass change at voltage above 1 V indicates the outflux of other species which cancels out the mass increase induced by the influx of Zn^{2+}. The only possible species in this case is OTf^- which carries the opposite charge as that of Zn^{2+}. We will show more evidence of OTf^- participating the reaction using FTIR in later session. The involvement of anions in the electrode reaction especially at voltage higher than 1.0 V indicates partial p-doping of PBQS. Since the quinone unit in PBQS is not known as p-dopable, the thioether linker is a possible redox center for p-doping. The molar ratio of OTf^- relative to Zn^{2+} is calculated to be 0.22 based on the overall mass change and the charges the ions carry.

Cyclic voltammetry cycling generated similar observation as observed above. The reversible frequency change (Fig. 2d) and overlapping of CV curves (Fig. 2e) during the initial five cycles indicate excellent reversibility, except the first cycle to be discussed later in Fig. 4. Figure 2f shows $\Delta f/n$ (n = 3, 5), ΔD, and voltage profile of the 5th cycle. Because $\Delta f/n$ overlaps with each other and ΔD is close to zero, $\Delta f/n$ can be analyzed with a gravimetric model. $F_{Faraday}$ is shown in Fig. 2f, following the Sauerbrey equation

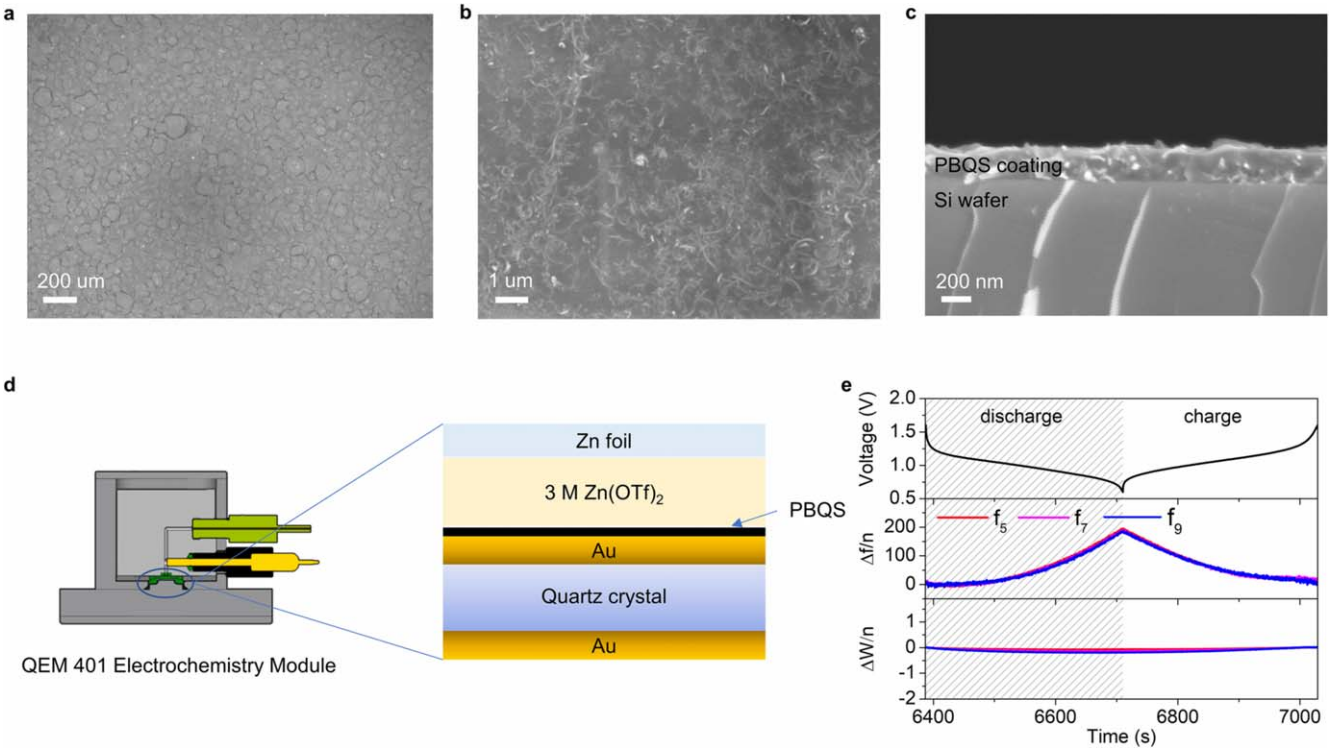

Figure 1. (a)–(b) SEM images for a spray-coated PBQS electrode on a gold sensor at different magnification. (c) A cross-sectional SEM image shows the thickness of a PBQS electrode coated on Si wafer prepared at the same condition. (d) Schematics of an EQCM-D cell configuration in this study. (e) Normalized changes of frequency ($\Delta f/n$) and resonance width ($\Delta W/n$) on multiple overtones (n = 5, 7, 9) during a discharge/charge cycle.

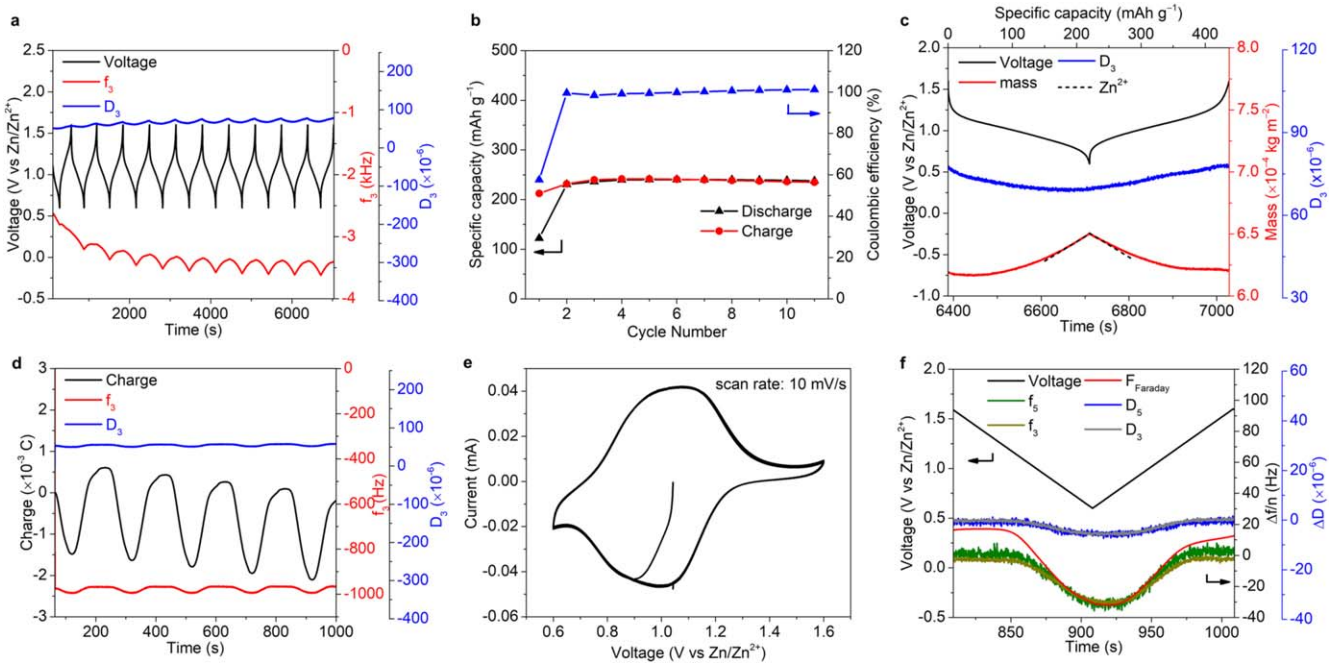

Figure 2. (a) The voltage profile and EQCM-D responses of a PBQS electrode tested in a 3 M $Zn(OTf)_2$ electrolyte at galvanostatic current of 50 μA (12 C) for 11 cycles. (b) The specific capacity and coulombic efficiency during the 11 cycles. (c) Voltage, mass, and 3rd order dissipation at the 11th cycle. Dashed Zn^{2+} line was calculated on the basis of Faraday's law, where the mass-per-charge ratio is 0.337 mg C^{-1}. (d)–(e) CV curves for 5 consecutive cycles at the scan rate of 10 mV s^{-1} and corresponding charge profile and EQCM-D responses. (f) The normalized change of frequency ($\Delta f/n$) and dissipation (ΔD) by the overtone order n ($n = 3, 5$) of the 5th CV cycle.

$F_{Faraday} = -\Delta m/C$, where C is the mass sensitivity constant of 17.7 ng/(cm^2 Hz) for a 5 MHz crystal, and Δm is mass change corresponding to Zn^{2+} ions by integrating CV curves using the Faraday law.[19] Similar to what we observed from galvanostatic cycling, Fig. 2f shows a voltage-dependent behavior—$\Delta f/n$ coincides with $F_{Faraday}$ only when voltage is lower than 1 V. Above 1 V, participation of OTf^- anion leads to deviation of $\Delta f/n$ from $F_{Faraday}$.

To provide chemical insight on the reaction mechanism, a custom-made in situ FTIR cell was set up with the schematic shown in Fig. 3a. A free-standing PBQS electrode was pressed against a diamond window of the FTIR with a piece of stainless-steel mesh serving as the current collector. A glass fiber separator was used to isolate the PBQS electrode from the zinc anode. Figure 3b shows three FTIR spectra where the signal for OTf^-, O−D, and carbonyl group (C=O and the reduced form C−O) can be clearly discerned. The change of peaks absorbance was plotted against cycling time to study the evolution of functional groups during the electrochemical process. As shown in Fig. 3c, the absorbance for C=O gradually decreases from 0.176 to 0.151 while that for C−O increases from 0.175 to 0.188 during the discharge process, supporting carbonyl groups as the redox centers. The absorbance for OTf^- decreases from 0.735 to 0.721 during discharge and recovers to 0.736 during charge, which provides additional support of the participation of OTf^- in the overall redox reaction. The insertion of Zn^{2+} is thus accompanied by the release of OTf^-, leading to the lower-than-expected mass change at voltage over 1.0 V. The change of O−D peak is relatively minor, which reflects the finding from EQCM measurements that no obvious hydration of Zn^{2+} during the reaction of PBQS.

Co-participation of cations and anions in the electrode reaction was further supported from the first cycle study of a pristine PBQS electrode. Figure 4a shows, during the first discharge, the mass curve follows the theoretical value (black dotted line) of Zn^{2+} insertion. The difference with Fig. 2c is explained by the absence of anions in pristine electrode, under which circumstance the injected charge is solely compensated by Zn^{2+}. During the first charge, release of Zn^{2+} was accompanied by the insertion of OTf^-, resulting in a net mass increase. During the first charge, the molar ratio of OTf^- relative to that of Zn^{2+} was calculated to be 0.66. This value is noticeably greater than 0.22 calculated for the representative cycle shown in Fig. 2c, indicating trapping of $Zn(OTf)_2$ in quinone polymers takes place during the first charge step. The proposed reaction mechanism was confirmed in multiple samples (Figs. S1a–S1b and Table SI is available online at stacks.iop.org/JES/167/070558/mmedia), indicating a good reproducibility. When conducting the first cycle EQCM-D characterization in the CV mode (Fig. 4b), $F_{Faraday}$ coincides well with the experimental values of $\Delta f/n$ in the first negative scan, confirming the reduction is compensated purely by Zn^{2+}. In the positive scan, $F_{Faraday}$ gradually deviates from $\Delta f/n$, due to the insertion of OTf^- while releasing Zn^{2+}. The different first-cycle behavior is also reflected in coin cell tests. Figure 4c compares the first two cycles of a PBQS electrode tested in a coin cell. During the second discharge, an additional discharge plateau around 1.1 V becomes obvious, attributed to the additional p-doping process. Note that the first-cycle coulombic efficiency for the coin cell is higher than that for the EQCM-D cell due to a self-discharge issue we had with our EQCM-D cell assembly. From all the above discussion, the proposed electrode reaction can be written as following:

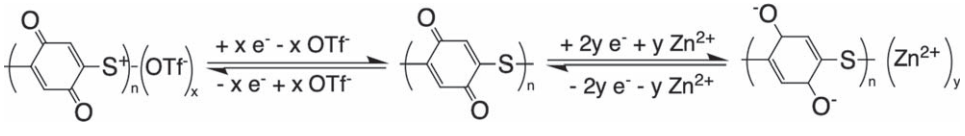

(1)

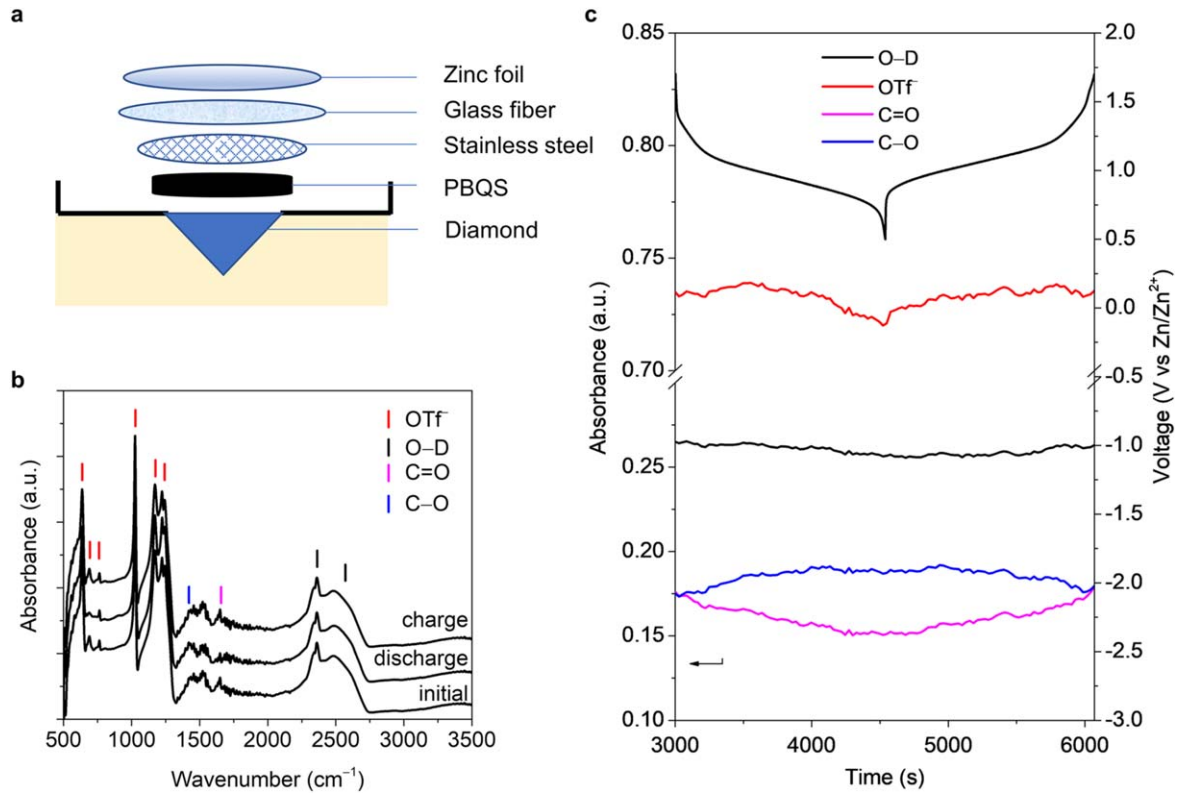

Figure 3. (a) Schematics of an in situ cell for FTIR characterization of PBQS electrode. (b) FTIR spectra of the initial state, discharged, and charged PBQS electrodes. The functional groups of interest are marked with colored lines. (c) The change of absorbance of selected peaks plotted against cycling time:–OD (2480 cm^{-1}), OTf^- (1026 cm^{-1}), –C=O (1631 cm^{-1}) and –C–O (1400 cm^{-1}).

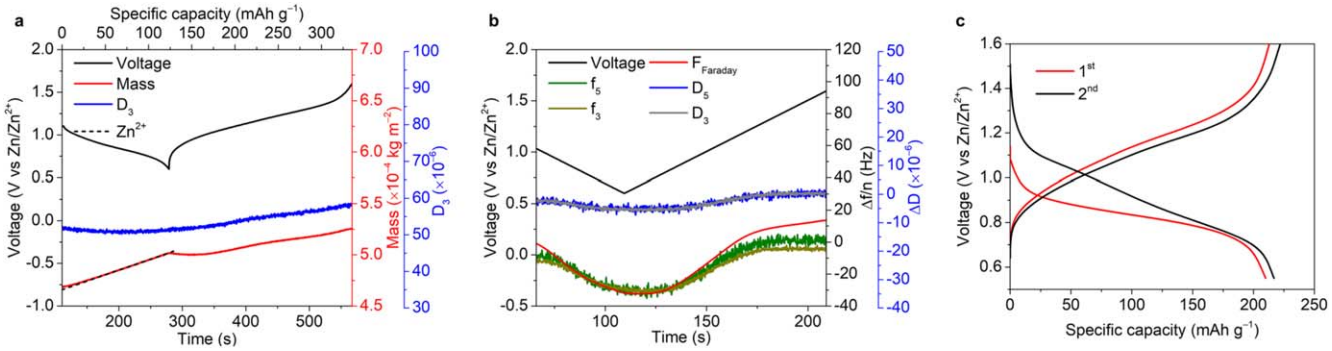

Figure 4. (a) Voltage profile and EQCM-D response measured during the first galvanostatic charge/discharge cycle. (b) Voltage profile and EQCM-D response measured during the first CV cycle. (c) The first two galvanostatic cycles of a coin cell at the current density of 400 mA g^{-1}.

Figure 5 shows the cycling performance of a PBQS-Zn coin cell at a current density of 400 mA g^{-1}. Except for the first discharge purely compensated by Zn^{2+}, the shape of voltage profile remains unchanged even after 1000 cycles, indicating a consistent and highly reversible charge storage mechanism. The capacity retention was 72% for 1000 cycles. The mechanism for the capacity decay is under investigation, and methods to improve the cycling stability is being developed.

Conclusions

In summary, for the first time, we have investigated the charge storage mechanism of a quinone polymer in a near-neutral zinc electrolyte solution with the combination of EQCM-D and in situ FTIR techniques. Zn^{2+} was found to be the cation species stored in the PBQS polymer with no obvious hydration. Triflate anion was also found to participate in the redox reaction at voltage above 1 V due to the unique thioether structure present in the polymer. We expect a fully Zn^{2+}-storage mechanism in quinone polymers without p-dopable redox groups like thioether. Our results indicate that quinone compounds have the potential to be the cathode materials for genuine aqueous zinc-ion batteries where the pH of the electrolyte solution remains unaltered during cell operation. We also show the combination of EQCM-D and FITR as a powerful tool for elucidating reaction mechanism of organic electrode materials.

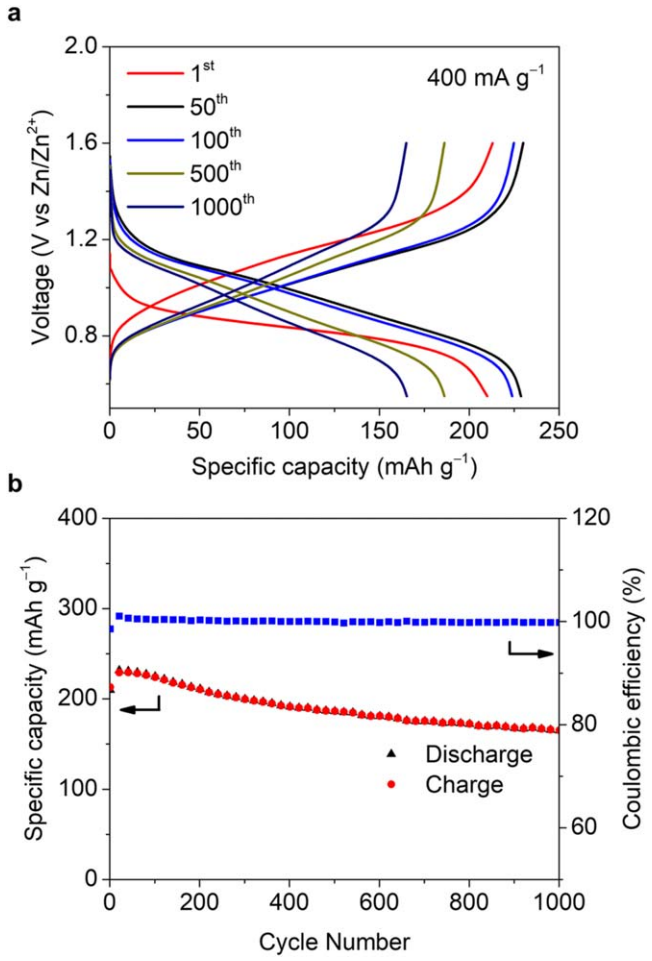

Figure 5. (a) Voltage profiles of the 1st, 50th, 100th, 500th and 1000th cycle of a PBQS electrode in a 3 M $Zn(OTf)_2$ electrolyte at a current density of 400 mA g^{-1}. (b) Specific capacity vs cycle number and corresponding coulombic efficiency.

Acknowledgments

This work was supported by TcSUH funding. We thank Prof. Yandi Hu and Meng Wang for the use of QCM-D instrument and assistance during the measurements. We thank Bin Wang for the assistance in the FTIR measurements.

Appendix

Typical voltage profiles and EQCM-D spectra of PBQS electrodes with different mass and calculated $\Delta m/e$ values are listed in the appendix.

ORCID

Ye Zhang https://orcid.org/0000-0001-7897-7485
Yanliang Liang https://orcid.org/0000-0001-6771-5172
Yan Yao https://orcid.org/0000-0002-8785-5030

References

1. G. Fang, J. Zhou, A. Pan, and S. Liang, *ACS Energy Lett.*, **3**, 2480 (2018).
2. M. Song, H. Tan, D. Chao, and H. J. Fan, *Advanced Funcitonal Materials*, **28**, 1802564 (2018).
3. A. Konarov, N. Voronina, J. H. Jo, Z. Bakenov, Y.-K. Sun, and S.-T. Myung, *ACS Energy Lett.*, **3**, 2620 (2018).
4. W. Sun et al., *JACS*, **139**, 9775 (2017).
5. H. Pan et al., *Nat. Energy*, **1**, 16039 (2016).
6. D. Kundu, B. D. Adams, V. Duffort, S. H. Vajargah, and L. F. Nazar, *Nat. Energy*, **1**, 16119 (2016).
7. Y. Liang, Y. Jing, S. Gheytani, K.-Y. Lee, P. Liu, A. Facchetti, and Y. Yao, *Nat. Mater.*, **16**, 841 (2017).
8. Y. Liang and Y. Yao, *Joule*, **2**, 1690 (2018).
9. Y. Jing, Y. Liang, S. Gheytani, and Y. Yao, *Chem. Sus. Chem.* (2020).
10. G. Dawut, Y. Lu, L. Miao, and J. Chen, *Inorganic Chemistry Frontiers*, **5**, 1391 (2018).
11. Q. Zhao, W. Huang, Z. Luo, L. Liu, Y. Lu, Y. Li, L. Li, J. Hu, H. Ma, and J. Chen, *Sci. Adv.*, **4**, eaao1761 (2018).
12. Z. Guo, Y. Ma, X. Dong, J. Huang, Y. Wang, and Y. Xia, *Angew. Chem. Int. Ed.*, **57**, 11737 (2018).
13. D. Kundu, P. Oberholzer, C. Glaros, A. Bouzid, E. Tervoort, A. Pasquarello, and M. Niederberger, *Chem. Mater.*, **30**, 3874 (2018).
14. W.-Y. Tsai, P.-L. Taberna, and P. Simon, *JACS*, **136**, 8722 (2014).
15. S. Wang, F. Li, A. D. Easley, and J. L. Lutkenhaus, *Nat. Mater.*, **18**, 69 (2019).
16. N. Shpigel, M. D. Levi, S. Sigalov, L. Daikhin, and D. Aurbach, *Acc. Chem. Res.*, **51**, 69 (2018).
17. Z. Song, Y. Qian, T. Zhang, M. Otani, and H. Zhou, *Advanced Science*, **2**, 1500124 (2015).
18. V. Dargel, N. Jäckel, N. Shpigel, S. Sigalov, M. D. Levi, L. Daikhin, V. Presser, and D. Aurbach, *ACS Applied Materials & Interfaces*, **9**, 17664 (2017).
19. N. Shpigel, S. Sigalov, M. D. Levi, T. Mathis, L. Daikhin, A. Janes, E. Lust, Y. Gogotsi, and D. Aurbach, *Joule*, **2**, 988 (2018).
20. N. Shpigel et al., *Nat. Mater.*, **15**, 570 (2016).
21. N. Shpigel, M. R. Lukatskaya, S. Sigalov, C. E. Ren, P. Nayak, M. D. Levi, L. Daikhin, D. Aurbach, and Y. Gogotsi, *ACS Energy Lett.*, **2**, 1407 (2017).
22. M. D. Levi, N. Levy, S. Sigalov, G. Salitra, D. Aurbach, and J. Maier, *JACS*, **132**, 13220 (2010).
23. M. D. Levi, G. Salitra, N. Levy, D. Aurbach, and J. Maier, *Nat. Mater.*, **8**, 872 (2009).
24. N. Shpigel, M. Levi, and D. Aurbach, *Energy Storage Mater.*, **21**, 399 (2019).